



<http://jaet.journals.ekb.eg>

## Modeling and Energy Analysis of the Hybrid Performance of Solar Dish Concentrator Integrated with Multi-Effect Desalination Unit

Moustafa M.Aboelmaaref<sup>a,b\*</sup>, Jun Zhao<sup>a</sup>, Mohamed E. Zayed<sup>c</sup>, Wenjia Li<sup>a</sup>, Ashraf Mimi Elsaid<sup>d</sup>,

Alaa A. Mahmoud<sup>e</sup>, M. Salem Ahmed<sup>b</sup>

(a) Key Laboratory of Efficient Utilization of Low and Medium Grade Energy, MOE, Tianjin University, Tianjin 300350, China.

(b) Mechanical Department, Faculty of Technology and Education, Sohag University, Sohag, 82524, Egypt.

(c) Mechanical Power Engineering Department, Faculty of Engineering, Tanta University, Tanta 31521, Egypt.

(d) Refrigeration and Air Conditioning Department of Technology, Faculty of Technology and Education, Helwan University, Cairo 11282, Egypt.

(e) Electrical Department, Faculty of Technology and Education, Sohag University, Sohag, 82524, Egypt.

\*Corresponding Author E-mail: mustafa\_mahmoud@techedu.sohag.edu.eg

### Abstract:

In this study, a hybrid commercial solar dish concentrator (SDC) integrated with a multi-effect distillation (MED) unit is thermodynamically modeled for the desalination process. A mathematical model implemented in MATLAB software is developed to simulate the proposed SDC/MED system to analyze its performance under the conditions of Tianjin (TJ), China. An energy analysis viability for assessing the life cycle of the SDC/MED system is also performed. The results demonstrated that, despite the site's solar radiation changes throughout the day, the desalinated water output for the proposed SDC/MED system is sufficient. In addition, the TJ-SDC/MED system is more cost-efficient than comparable standalone desalination systems. The simulation of the SDC with the MED unit of five effects yielded average productivity of roughly 95.5 kg/s, a specific cooling water flow rate of 1.689, and an overall performance ratio of 223.3. It is recommended that the hybrid SDC/MED system is an efficient choice for producing potable water in large scale desalination applications.

**Keywords:** Multi-effect desalination; Solar dish concentrator; Energy analysis; Freshwater production; Overall efficiency; Case study.

### Nomenclature

#### Symbols

$A_{con.}$	Aperture area of the dish, $m^2$
$A_{o,cav.}$	Cavity outer area, $m^2$
$C_{gD}$	Design geometric concentration
$D_{cav.}$	Diameter of the cavity, m
$D_{fi}$	Tube inner diameter, m
$D_{fo}$	Tube outer diameter, m
$F_D$	Degradation factor
$Gr$	Grashof number
$h_{conv., forced}$	Forced convection, $W/m^2.K$
$h_{conv., natural}$	Natural convection, $W/m^2.K$
$h_{ext,cav.}$	Receiver external convection, $W/m.K$
$I_{Bn}$	Direct normal irradiation, $W/m^2$
$k_{amb}$	Thermal conductivity of air, $W/m.K$

#### Greek Symbols

$\sigma$	Steven Boltzmann constant ( $5.67 \times 10^{-8}$ , $W/m^2.K^4$ )
$\eta_c$	Concentrator efficiency
$\xi_{ff}$	Effective absorbance of receiver
$\rho_m$	Concentrator mirror reflectivity
$\Gamma$	Solar interception factor
$\gamma$	Receiver tilt angle
$V_w$	Wind speed, m/s
<b>MED System</b>	
$A$	Area of heat transferred, $m^2$
$B$	Flow rate of Brine each effect, g/s
BPE	Boiling point elevation, $8^\circ C$
$C_p$	Specific heat seawater capacity at constant pressure, $kJ/kg.^{\circ}C$
$D$	Distillate flow rate by boiling for each

$k_{ins}$	Insulation thermal conductivity, W/m.K	$D_f$	Distillate flashing flow rate for each flashing box, g/s
$k_{rec}$	Receiver thermal conductivity, W/m.K	F	Feed flow rate to each effect, g/s
$L_{ins}$	Insulation thickness, mm	GR	Gain ratio
$r_r$	Recovery ratio, %	h	Heat transfer coefficient, W/m <sup>2</sup> .°C
Re	Reynold's number	L	Heat of latent, kJ/kg
$Q_{cond.}$	Conduction heat loss, W	LMTD	Temperature difference by logarithmic mean approach, °C
$Q_{conv.}$	Convection heat loss, W	$\dot{m}$	Mass flow rate, kg/s
$Q_{loss}$	Total heat loss, W	n	Total number of effects
$Q_{rad}$	Radiation heat loss, W	$T_b$	Temperature of brine boiling in the effects, °C
$Q_{ref}$	Energy reflected, W	$T_c$	Cooling water temperature, °C
$Q_u$	Useful Energy, W	$T_f$	Feed temperature, °C
$T_{cav.}$	Cavitation receiver temperature, °C or K	$T_n$	Last effect temperature, °C
$Q_{loss}$	Total heat loss, W	$T_s$	Steam temperature, °C
$T_v$	Vapor temperature, °C	$\Delta T$	Temperature decreases, °C
S	Steam flow rate entering the first effect, g/s	$X_b$	Brine salinity
$U_e$	Evaporator section overall heat transfer coefficient, kW/m <sup>2</sup> .°C	$X_f$	Salt concentration, ppm or g/kg
$T_s$	Steam temperature, °C	y	Flashing fraction
$T_v$	Vapor temperature, °C	Subscripts	
$U_c$	Condenser section overall heat transfer coefficient, kW/m <sup>2</sup> .°C	1,2, ..... ,n	effect number
		c	condenser
		cw	cooling seawater
		v	vapor

## 1. Introduction

Important global challenges like water and energy are not being adequately addressed in the face of a growing population and advanced technology, causing great concern for scientists and decision-makers. Important global challenges like water and energy are not adequately addressed in the face of a growing population and advanced technology, causing great concern for scientists and decision-makers. This is due to the depletion of both fossil fuel and drinkable water. Therefore, it was necessary and crucial to create a sustainable, clean, and viable energy source using desalination techniques. The present global energy transformation must include solar energy. Since solar energy is free and plentiful, it

is becoming more competitive with conventional fossil fuels, which produce significant amounts of greenhouse gases.

Freshwater scarcity is one of the most urgent problems facing the globe today because of the rapid industrial and population growth, even while new technologies are being employed to produce and store solar energy.

Desalination as a viable alternative for supplying freshwater is gaining popularity in this area. A combination of desalination and renewable energy technologies may help to mitigate these negative consequences to some degree [1,2]. Therefore, by linking it, solar energy is used for power production or heating source for seawater desalination methods such as reverse osmosis and multi-effect evaporators [3-9]. Although the reverse osmosis technique has the highest

freshwater production, it consumes much power [10-20]. This requires finding other sources for desalination of seawater with low energy and relatively high productivity.

Systems producing water using multi-effect evaporation and humidification-dehumidification (HDH) water desalination use less energy. The most efficient and effective solar concentrator devices in engineering applications include the linear Fresnel reflector (LFR), a parabolic trough collector (PTC), solar towers, and solar dishes [21–26]. Sunlight is captured by solar dish concentrators, which turn it into heat to heat water, which is then utilized as a source of heat for the multi-effect evaporator [27-29]. The effectiveness of the Stirling engine based on a dish concentrator for the creation of electric power has also been studied. A solar dish/Stirling engine system (SDSES) with a rated output of 25 kW was the subject of a thermodynamic theoretical model and a techno-economic study conducted by Zayed et al. [30]. According to the results, the system generates 3.5 MWh of energy each month at a maximum efficiency of 22.75% and 28.748 MWh yearly at a net overall efficiency of 19.55%. Zayed et al. [31] looked at how the SDSES's output power and overall efficiency were affected by the concentrator diameter, receiver operational temperature, DNI, wind speed, and ambient temperature. The results manifested that the SDSS's power production and overall efficiency rise with increasing DNI and receiver temperatures while decreasing with increasing ambient temperatures and wind speeds.

From the literature review, an energy-efficient standalone desalination unit such as the MED system powered by solar energy that may be used in distant areas to cover the needs of desalinated water is urgently needed.

To do this, the performance of the hybrid SDC/MED system is studied using the simulation code of MATLAB. The theoretical model, design, and operational conditions of Tianjin city-China are included in the present research.

The proposed strategy in this study is to develop a hybrid standalone solar-powered desalination system with two subsystems making up the proposed system. The first one is the solar dish concentrator (SDC), which supplies steam to the MED unit. The MED system for the desalination stage is the second system with five effects. A commercial code of MATLAB software is used to simulate the hybrid system MED/SDC. A schematic of the freestanding MED unit powered by the solar dish concentrator is shown in Fig. 1.

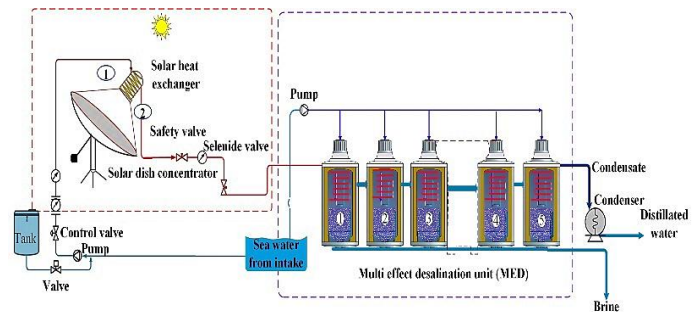


Figure 1. sketch diagram for the mechanism of the TJ-SDC/MED system.

**2. Methodology**

The proposed model solves the mass and energy balance of the hybrid system using MATLAB software. Temperature and water salinity are entered as parameter values; however, brine salinity and the temperature of the ultimate effect are ignored. Two codes have been developed for the proposed hybrid system: one for the multi-effect evaporation desalination (MED) system equations and the other for the solar dish concentrator (SDC). The model result is used to compute the performance respect ratio, specific heat transfer surface area, and specific cooling water flow rate for the system. The results include impact temperatures, distillate flow, and brine flow.

**2.1 Configuration of the solar dish concentrator (SDC)**

SDC is a focused solar technology that converts solar energy into thermal energy by concentrating radiation on the receiver from the solar collector. Figure 2 shows the system heat balance of the SDC, and Table 1 demonstrates the design specifications of the SDC system. The heat is absorbed by the circulated water flowing through a cylindrical coil (a cavity receiver), as shown.

The solar dish includes mirror reflection (reflectivity 0.92). In the solar thermal receiver, a hollow copper cylindrical coil was placed in the focal zone of the solar dish. A solar dish concentrator with a solar thermal receiver was employed to heat and raise feed water temperature before pumping to the MED unit in the proposed unique hybrid system of SDCs driven MED desalination unit combined with a solar dish concentrator. Table 1 shows the dimensions of each component of the proposed hybrid system of an SDC-driven MED desalination unit coupled with a solar dish concentrator.

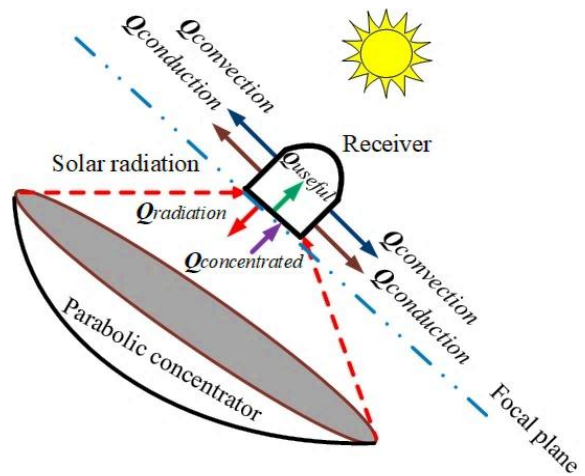


Figure 2. Receiver’s of the energy distributed in the SDCs.

Table 1. Design and operation data of the proposed hybrid model.

Parabolic dish	Specifications
Dish diameter (m)	12.5
aperture area (m <sup>2</sup> )	122.72
Effective aperture area (m <sup>2</sup> )	105
Mirror reflectance	0.92
Total optical error	8
Tracking system	Altitude, azimuth tow axis
Type	Paraboloid

No. of mirror units	144
Tracking control	Open circuit
Cavity reciever design with Tianjin solar dish concentrator (TJ-SDC/MED):	
Type	Cylindrical cavity
Aperture diameter (m)	0.25
Pipe outer diameter (m)	0.035
Pipe inner diameter (m)	0.0326
Pipe length (m)	25.4
Number of coils	12

### 2.1.1 The mathematical model

The analysis model of the TJ-SDC was conducted to evaluate the performance of the new design of the SDC for supplying the heating energy to the MED desalination unit.

#### A. Thermal analysis model of both receiver and reflector cavity:

As illustrated in Figure 2, a thermodynamic analysis model was utilized to calculate the parabolic and receiver system's output energy and total heat efficiency. The difference between the power reflected by the parabola to the receiver ( $Q_{rec}$ ) and the total heat loss ( $Q_{loss}$ ) is known as the usable energy in the cavity ( $Q_u$ ), which is defined as the energy obtained by the working fluid:

$$Q_u = Q_{rec} - Q_{loss} \quad (1)$$

Where  $Q_{rec}$  and  $Q_{loss}$  denote the energy reflected by the dish to the receiver and the total heat losses, respectively. The reflected power to the receiver is given by Eq. (2) [27].

$$Q_{rec} = \rho_m \Gamma I_{Bn} A_{con} \quad (2)$$

Where  $\rho_m$  represents the concentrator mirror reflectivity is 0.92 [28] and  $\Gamma$  the sun interception factor. This factor is assumed between 0.9 and 0.99, according to the Harrigan model [29, 30]. Further, in this paper for the possibility of maximum losses, ( $\Gamma$ ) is assumed 0.9. ( $I_{Bn}$ ) is the direct normal irradiance,  $W/m^2$ .

#### B. The receiver's total heat losses

Determination of the gross thermal loss of the receiver is accomplished by the value of three types of thermal losses in the receiver: convection, conduction, and radiation [21].

$$\dot{Q}_L = \dot{Q}_{conduction} + \dot{Q}_{convection} + \dot{Q}_{radiation} \quad (3)$$

Firstly, the thermal loss via radiation " $\dot{Q}_{radiation}$ " is given by the following equation [31-33]

$$\dot{Q}_{rad} = \varepsilon_{eff} \cdot A_{cav} \cdot (T_{cav}^4 - T_{amb}^4) \quad (4)$$

$$\text{Where } \varepsilon_{eff} = \frac{1}{\left[1 + \left(\frac{1}{\varepsilon_c} - 1\right) \frac{A_{ap}}{A_{cav}}\right]} \quad (5)$$

$T_{\infty}$ = ambient temperature,  $T_{cav}$ = cavity receiver temperature.

The (cavity receiver temperature) " $T_{cav}$ ", is given as [34,35].

$$T_{cav} = \sqrt[4]{\frac{\alpha_{abs,r} C_{g,D} I_{Bn}}{\sigma \varepsilon_r}} \cdot \xi_{att} \quad (6)$$

Where  $C_{g,D}$  design geometric concentration and the receiver temperature near to the working temperatures is provided as: " $\xi_{att}$ " is an attenuation constant, while the transmitter temperature is given as:

$$\xi_{att} = \eta_c F_D F_{EX} \quad (7)$$

Where  $\eta_c$  efficiency of the concentrator and  $F_D$  (degradation factor),  $F_{EX}$  (Excess heat removal factor).

The parabolic concentrator efficiency  $\eta_c$  may be computed using the concentrator mirror characteristics and manufacturing process defects, as shown in [36].

$$\eta_c = \rho_m F_{sh} \Gamma \quad (8)$$

$F_{sh}$  stands for the un-shading factor. The natural convection thermal loss within the cavity receiver " $Q_{conv,nat}$ " and the power convection thermal loss owing to wind speed " $Q_{conv,wind}$ " make up the convective thermal loss " $Q_{conv}$ ". The natural convection thermal loss ( $Q_{conv,nat}$ ) within the cavity receiver may be computed as follows:

$$Q_{conv} = (h_{conv,nat} + h_{conv,forced}) A_{cav} (T_{cav} - T_{\infty}) \quad (9)$$

The heat convective “ $h_{conv,nat}$ ” is determined by the cavity insulation and receiver diameters, the thermal losses conductivity of the receiver material, the receiver tilt angle, and the temperature of the cavity receiver and its surroundings. It may be determined in the following way [37].

$$h_{conv,nat} = \frac{K_{rec}}{D_{rec}} \left[ 0.088 \cdot Gr^{0.333} \cdot \left(\frac{T_{cav}}{T_{\infty}}\right)^{0.18} \cdot (\cos\gamma)^{2.47} \cdot \left(\frac{D_{rec}}{D_{cav}}\right)^{1.12} Q_{cond}^{0.98} \left(\frac{D_{rec}}{D_{cav}}\right) \right] \frac{(T_{cav} - T_{\infty})}{\frac{\ln \frac{D_{ro}}{D_{ri}}}{2\pi K_r L_r} + \frac{\ln \frac{D_{cav}}{D_{ro}}}{2\pi K_{ins} L_{ins}} + \frac{1}{h_{ext,cav} A_{o,cav}}} \quad (10)$$

Where  $\gamma$  is tilt angle of the receiver, ( $K_{rec}$ ) is the receiver thermal conductivity, W/m.K and ( $Gr$ ) Grashof number.

The receiver tilt angle ( $\gamma$ ) and wind speed ( $v_w$ ) affect forced convective thermal loss ( $h_{conv,forced}$ ) as follows [38,39]:

$$h_{conv,forced} = f(\gamma) \cdot v_w^{1.401} \quad (11)$$

Where  $f(\gamma)$  is dependent according to ref. [39] as:

$$f(\gamma) = 0.1634 + 0.7498 \sin \gamma + 0.5026 \sin 2\gamma + 0.3278 \sin 3\gamma \quad (12)$$

Where “ $\gamma$ ” is the inclination angle of the cavity receiver on the horizontal plane, and it is adjusted at  $75^\circ$  [36], resulting in minimal wind convection thermal loss.

The heat loss by conduction “ $Q_{cond}$ ” is computed as [40,41]

$$Q_{cond} = \frac{(T_{cav} - T_{\infty})}{\frac{\ln \frac{D_{ro}}{D_{ri}}}{2\pi K_r L_r} + \frac{\ln \frac{D_{cav}}{D_{ro}}}{2\pi K_{ins} L_{ins}} + \frac{1}{h_{ext,cav} A_{o,cav}}} \quad (13)$$

The receiver cavity external surface convection heat “ $h_{ext,cav}$ ” is estimated as [42]

$$h_{ext,cav} = 0.148 Re^{0.633} \frac{K_{\infty}}{D_{cav}} \quad (14)$$

Where  $K_{\infty}$  is the air thermal conductivity W/m.K

Fig. 3 illustrates the flow chart describing the SDC mathematical solution technique.

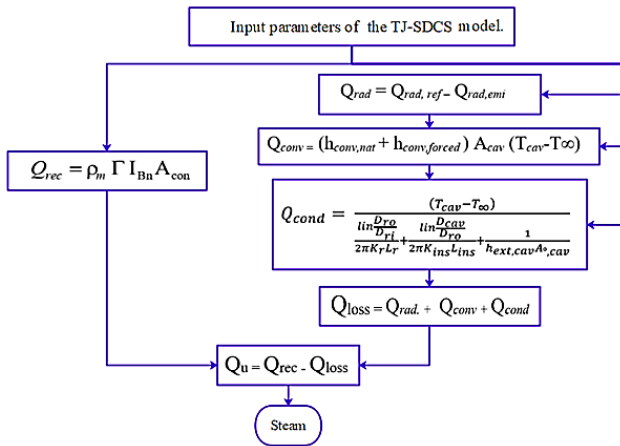


Figure 3. Flow chart of the SDC system.

## 2.2 MED desalination unit

In the current investigation, a parallel feed MED is explored, as illustrated in Fig. 3. A

multi-effect evaporation unit is made up of several single-effect evaporators. The first effect is heated by a source outside of the system, such as steam. Then, the vapor created in the previous effect heats the rest of the effects, preventing the heated brine from being rejected and, as a result, reducing energy loss. Many facilities in the desalination business use this technique. The unit can be used on its own or in conjunction with heat or mechanical vapor compression systems (MVC).

### 2.2.1 Working Principle

Figure 4 displays a multi-effects vaporization system using parallel feeds and

n-effects from the left while the stream flows ahead of the first effect. A heat transfer surface, a droplet separator, and a salt pool are all included in each effect. The vapor moves in the direction of dropping pressure and temperature for each effect, while the input sea water flows vertically. In addition, a condenser is at the down of the evaporators (the last effect, and (n-1) flash droplets, the feed saltwater is chemically treated. The feed seawater temperature rises to the boiling (saturation) point in each evaporator, then a portion of it evaporates. The steam inside tubes provides the heat required for preheating and evaporation in the first, effect. The system is powered by an external supply of steam. For all effects of raising the boiling point, the steam saturation temperature is lower than the boiling temperature of the brine (BPE). The steam passes through a demister or mist eliminator to remove the accompanying brine droplets. The amount of steam formed by one effect is greater than the amount of steam formed by the next effect. This is due to the fact that when the temperature drops, the latent heat of vaporization rises.

**2.3 Modeling of MED unit**

MATLAB software is used to model the MED plant. Table 2 and Table 3 show the Table 2. Inputs of the multi-effect desalination system model

Parameter	Symbol	Value
No. of effects	n	5
First effect temperature (°C)	T <sub>1</sub>	48
Last effect temperature (°C)	T <sub>n</sub>	68
Brine water temperature entering the condenser (°C)	T <sub>cw</sub>	33
Seawater temperature leaving the condenser (°C)	T <sub>f</sub>	45
Brine salinity entering the condenser (ppm)	X <sub>f</sub>	40,000
Motive steam temperature (°C)	T <sub>m</sub>	159
Motive vapor pressure (kPa)	P <sub>m</sub>	600
Recovery ratio (%)	rr	30% ≤ RR ≤ 40%

boxes. The latent heat of the condensing vapor from the previous effect is absorbed by feed seawater in the down condenser. As a result, its temperature rises to that of the feed saltwater To ensure that all the vapor formed in the back effect is condensed, a part of the heated saltwater is returned to the sea as cooling water. Before being sprayed into the evaporators in a form of small. model inputs and practical equations for this MED plant's mathematical model, respectively. The following simplification assumptions were used in this model [43]:

- All effects have a constant temperature differential, and the distillate is salt-free.
- The operation in a steady condition.
- In all effects, there is an equal feed flow rate.
- Minimal losses in thermodynamic analysis.
- Each impact has the same boiling point elevation of 1 °C.

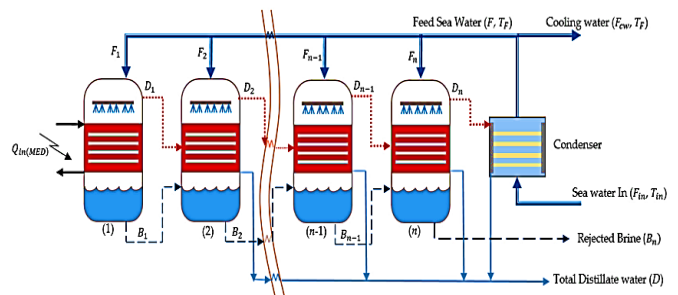


Figure 4. Parallel MED desalination unit.

Table 3. Governing equations of Mathematical analysis modeling of the MED unit

Definition	Equation
Temperature difference of effects, $\Delta T$ (°C)	$\Delta T = \frac{T_1 - T_n}{n-1}$
Compressed steam temperature, $T_s$ (°C)	$T_s = T_1 + \Delta T$
Effects steam temperature, $T_{v,i}$ (°C)	$T_{v,i} = T_i - \text{BPE}$
Mass, Energy, and salinity balance (for $i = 1, 2$ ) Condenser performance,	$D_1 = \frac{(D_m + D_{ev})\lambda_s - F_1 C_p (T_1 - T_f)}{\lambda_1}$
Distillated flow rate, $D_i$ (g/s)	$D_1 = \frac{D_1 \lambda_1 - F_2 C_p (T_2 - T_f) + B_1 C_p (T_1 - T_2)}{\lambda_2}$
Brine flow rate, $B_i$ (g/s)	$B_1 = F_1 - D_1, B_2 = F_2 + B_1 - D_2, B_i = F_i + B_{i-1} - D_i$
Salinity of brine, $x_i$ (ppm)	$X_1 = \frac{F_1}{F_1 - D_1} X_f, X_2 = \frac{X_f F_2 + X_1 B_1}{B_2}, X_i = \frac{X_f F_i + X_{i-1} B_{i-1}}{B_i}$
Distillate flow rate, $D_i$ (g/s)	$D_i = \frac{D_{i-1} + D_{fi}}{\left[1 + \frac{RC_p(T_i - T_f)}{L}\right]}$ for $i \neq 1$ [44]
$y =$ Flashing fraction	$D = \sum_i^n D_n, R = 3$
$L =$ Latent heat, kJ/g	$D_{fi} = y B_{i-1}$
$B =$ brine flow rate, g/s	$B_i = \sum (R - 1) D_i$ [44]
$F =$ Feed of flow rate, g/s	$B_1 = (R - 1) D_1$
$F_1 = 40$ g/s	
$K =$ Condenser effectiveness	$k = \frac{T_f - T_c}{T_{vn} - T_c}$
$T_c =$ Cooling water temperature, °C	

Where ( $A_i$ ) MED's each effect area ( $m^2$ ), ( $B$ ) salt permeability constant ( $kg/m^2.s$ ), ( $B_i$ ) brine flow rate out of multi effect all effect (g/s), ( $F_i$ ) feed water of MED's, each effect (g/s), ( $T_i$ ) temperature effect (°C).

( $T_{v,i}$ ) Saturated steam temperature for each effect (°C), ( $x_f$ ) MED water supply concentration (ppm), ( $X_i$ ) MED effect brine concentration (ppm), ( $\lambda_i$ ) evaporation enthalpy effect MED (kJ/kg).

The temperature difference between all effects is the same as the temperature difference between heated steam and vapour produced by the first effect. The temperature differential between the steam generated by the final effect and the temperature of the

The salinity in each effect is given by:

$$F_i \cdot X_f = B_i \cdot X_i \quad (17)$$

saltwater entering the down condenser is also significant.

$$\Delta T = T_s - T_{v1} = T_{v1} - T_{v2} = T_{v2} - T_{v3} = T_{v3} - T_{vn} = T_{vn} - T_c \quad (15)$$

The cooling water mass flow rate, (Energy balance at condenser) is given by the following equation:

$$\dot{m}_{cw} = \frac{\dot{m}_v L_c}{C_p (T_{cw} - T_{sw})} \quad (16)$$

Where:  $\dot{m}_v =$  Condenser vapor flow rate, g/s

$L_c =$  Condenser vapor latent heat, g/s

Energy balance in the first effect:

$$\dot{m}_s \cdot L_s = F_1 C_p (T_1 - T_f) + D_1 \cdot L_1 \quad (18)$$

Energy balance in each effect:

$$D_{i-1} \cdot L_{i-1} + D_{f,i-1} \cdot F_{i-1} = F_i C_p (T_i - T_f) + D_i \cdot L_i \quad (19)$$

The boiling point temperature (BPT) is given by:

$$\text{BPT} = X_i (B + C X_i) \times 10^{-3} \quad (20)$$

Where:  $B = [(6.71 + 6.34 \times 10^{-2} T_i) + (9.74 \times 10^{-5} T_i^2)] \times 10^{-3}$

$C = (22.238 + 9.959 \times 10^{-3} T_i + 9.42 \times 10^{-5} T_i^2) \times 10^{-8}$

The latent heat of vaporization is calculated by the following correlation:

$$L = 2501.897 + 2.41T + 1.19 \times 10^{-3} - 1.59 \times 10^{-5} T^3 \quad (21)$$

The vapor density is calculated by the following correlation:

$$\rho_v = 0.0051 + 0.00024 T_v + 1.8 \times 10^{-5} T_v^2 - 4.33 \times 10^{-8} T_v^3 + 4.34 \times 10^{-9} T_v^4 \quad (22)$$

Condenser overall convection heat transfer is estimated by the following correlation:

$$A_i = \frac{D_{i-1} L_{i-1}}{U_i (T_{vi-1} - T_i)} \quad (27)$$

The condenser heat transfer area can be computed as follows

### 2.4 Performance of MED system

The performance ratio (PR) is a term used to describe the performance of multi effect desalination systems, which are similar to thermal desalination systems. It's calculated as the ratio of the system's produced water

$$U_{\text{cond}} = 1.72 + 3.21 \times 10^{-3} T_v - 1.6 \times 10^{-5} T_v^2 - 1.99 \times 10^{-7} T_v^3, \text{ kW/m}^2 \cdot \text{K} \quad (23)$$

For each evaporator effect, the overall heat transfer convection is computed by the following correlation:

$$U_E = 1.97 + 1.2 \times 10^{-3} T_b - 8.598 \times 10^{-5} T_b^2 - 2.57 \times 10^{-7} T_b^3, \text{ kW/m}^2 \cdot \text{K} \quad (24)$$

The saturated temperature is calculated using the following correlation:

$$\ln(P_{\text{sat}}/P_c) = \left( \frac{T_c}{T + 273.15} - 1 \right) \sum_{i=1}^8 f_i (0.001 (T + 273.15 - 338.15))^{i-1} \quad (25)$$

$T_c = 647.286 \text{ K}$  and  $P_c = 22089 \text{ kPa}$

$f_1$	$f_2$	$f_3$	$f_4$
-7.416242	0.29721	-0.1155286	0.008685635
$f_5$	$f_6$	$f_7$	$f_8$
0.001094098	-0.00439993	0.002520658	-
			0.000521868

The heat transfer area of evaporators for the parallel MED can be calculated as follow:

For the first effect:

$$A_1 = \frac{Q_{in(MED)}}{U_1 (T_s - T_1)} \quad (26)$$

For the effect 2-n:

$$A_c = \frac{D_n L_n}{U_c (LMTD)_c} \quad (28)$$

$$(LMTD)_c = \frac{T_{in} - T_F}{\ln \left[ \frac{T_{vn} - T_F}{T_{vn} - T_{in}} \right]} \quad (29)$$

flow rate to its vapor consumption flow rate [45].

$$PR = \frac{\dot{m}_d}{\dot{m}_s} \quad (30)$$

Where:  $\dot{m}_d$  = The amount of permeated produced in g/s.

$\dot{m}_s$  = The amount of entering vapor in g/s.

The specific cooling water flow rate is given by:

$$s\dot{m}_{cw} = \frac{\dot{m}_{cw}}{\dot{m}_d} \quad (31)$$

The specific heat transfer of a surface area is given by:

$$S_A = \frac{\sum_{i=1}^n A_i + A_c}{\dot{m}_d} \quad (32)$$

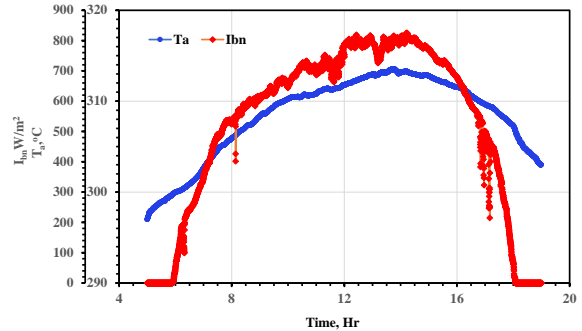
### 3. Results and discussion

In this section, the findings of numerical modeling of the solar desalination system consisting of a solar dish concentrator and a multi-effect desalination unit are presented for the climatic conditions of Tianjin, China. A group of influencing factors such as the effect of changing the outside air temperature, the intensity of solar radiation, and time was studied to verify the extent of their impact on the performance of the solar desalination system. The next part is divided into two subsections to display the results of numerical modeling using the MATLAB program for both the solar dish collector and a multi-effect desalination unit.

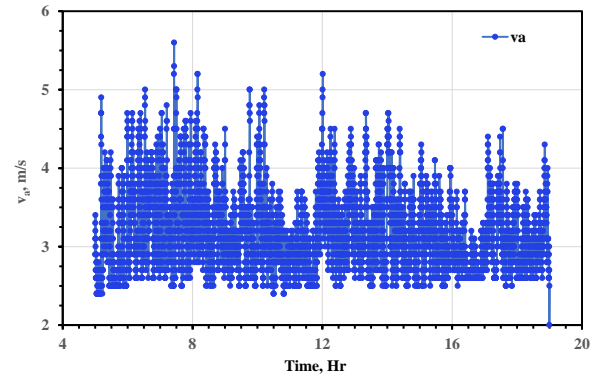
#### 3.1 Environmental Conditions

The meteorological conditions for the period recorded in Tianjin, China, are depicted in the following curves, which are essential to the theoretical study of the simulated system. Figure 5a shows the variation of solar intensity at Tianjin, China during the daytime. Figure 5b also shows the distribution of ambient temperature and wind speed. From 5:00 a.m. to 19:00, fluctuations in ambient air temperature, direct sun intensity, and wind speed were recorded for Tianjin, China (39.3434° N and 117.3616° E). Figure 5a shows that the intensity of solar radiation increases between 5 am and 7 pm and decreases until it reaches its maximum of 830 W/m<sup>2</sup> at 2

a.m. Also, within this period, the temperature ambient varied between 33 and 39 °C and 24–40 °C over the day. Furthermore, as shown in Fig. 5b, the wind speed data for Tianjin city has an average value of 3.3 m/s. It is apparent that the wind speed varies during the day depending on temperature and solar intensity.



(a) Variation of ambient temperature and solar radiation distribution during daytime



(b) Wind speed distribution during the daytime

Figure 5. Variation of solar radiation, ambient temperature, and wind speed during daytime at Tianjin, China.

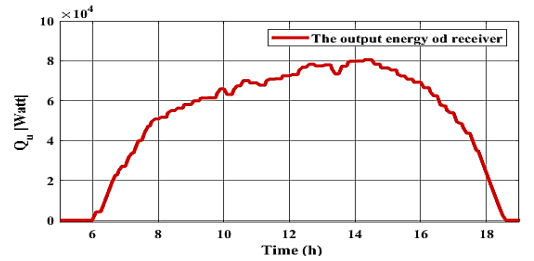
#### 3.2 Useful energy generated from the SDC

Figure 6. shows the net useful energy generated by the SDC as a result of solar radiation falling on the reflectors and collected on the receiver at the SDC focus during the day considering losses. When the

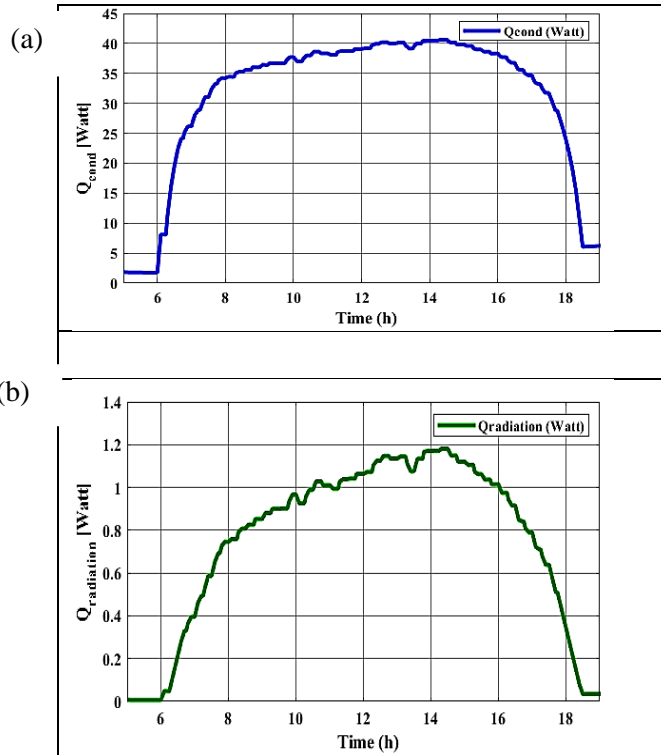
amount of solar radiation reaches a rising level of over,  $800 \text{ W/m}^2$  at 2:00 pm, the effective heat output of the receiver also

Solar thermal concentrators absorb sunlight and concentrate it on a receiver, boosting the temperature by hundreds of degrees and enabling high-value energy conversions. When operating at high temperatures, the receiver's performance diminishes as a result of increased heat losses. The losses included conduction, convection, and radiation. As shown in Fig. 7a, the quantity of energy conduction through the receiver increases with time, reaching a peak of 41 W between 10 and 2 p.m. (peak period), then it declines to the lowest value after 6 p.m. due to a decrease in the intensity of direct solar radiation during the day. Similarly, the amount of heat radiation through the receiver increases to a maximum value of 1.2 W at 2 o'clock as seen in Fig. 7b. The value of the radiation heat decreases sharply until it reaches a minimum value with the decrease in the intensity of solar radiation during the day. Figure 7c shows the relationship between the amount of heat convection with time during the period from 5 a.m to 7 p.m for the city of China. The convection heat rate of the concentrator receiver rises to a maximum value of 2750 W until 2 p.m during afternoon period from 11 p.m to 3 p.m, after which the convection heat drops sharply according to the decrease in wind speed and the decrease in the rate of solar radiation at the end of the day.

increases to a certain value called a maximum of  $8.1 \times 10^4 \text{ W}$  and then decreases rapidly with time at lower solar intensity.



Also, Fig. 7d confirms the relationship between total heat losses (conduction, convection, and radiation) and time, displaying the same curve direction for the same result, indicating that the peak time of 2 p.m. results in the highest total heat loss of 2780 W.



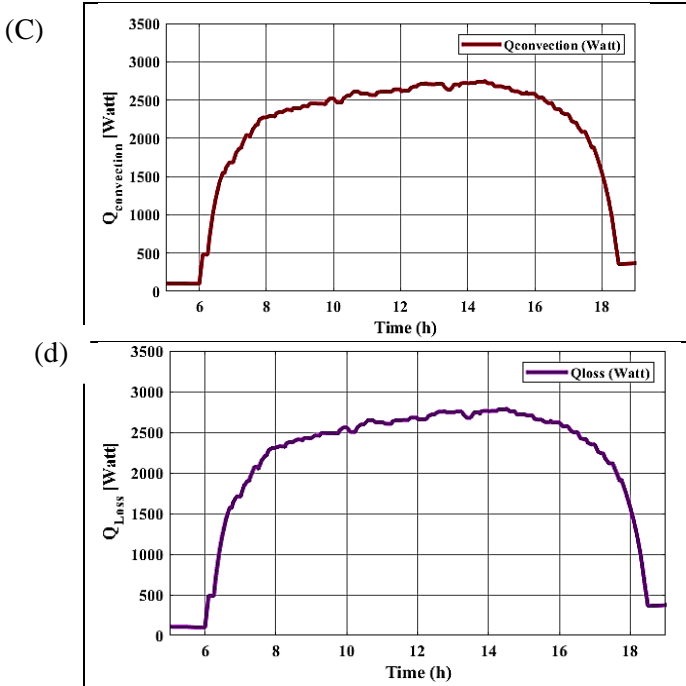


Figure 7. Hourly variation of the receiver heat losses during daytime: (a) Hourly variation of conduction a heat loss; (b) Hourly variation of radiation a heat loss; (c) Hourly variation of convection heat loss; (d) Hourly variation of total heat loss.

Figure 8a shows the hourly compound efficiency from 5 a.m to 7 p.m for China city. The trend indicates that the maximum efficiency is 82%, which is recorded at 14:00 p.m. In the afternoon, compound efficiency decreases as solar radiation decreases, and therefore the productivity rate decreases accordingly. The variation between efficiency and useful heat rate is illustrated in Fig. 8b. It can be seen from the figure that the receiver concentrator efficiency is increased with the increase of the useful heat rate.

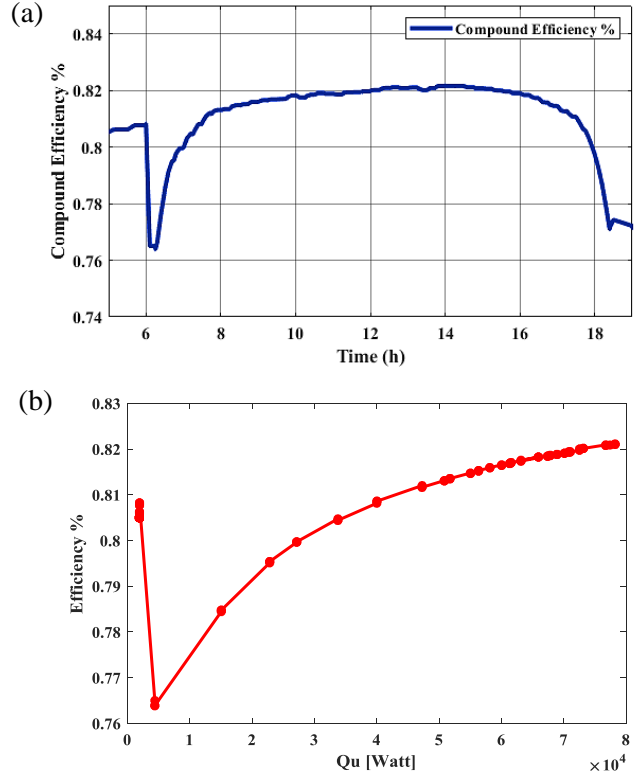


Figure 8. (a) Hourly variation of total overall efficiency versus time; (b) Variation of overall efficiency versus useful energy

On the other hand, Fig. 9 displays a representation of the convection and radiation heat rate of the receiver versus solar intensity for a constant ambient temperature of 298 K and wind speed of 2.5 m/s. The figure shows that the receiver heat convection and heat radiation rate increase for all sun irradiance values. The intensity rate of the sun is an important factor influencing the heat transfer rate by convection and radiation of the receiver which depends on the latitude and geographic location of the city.

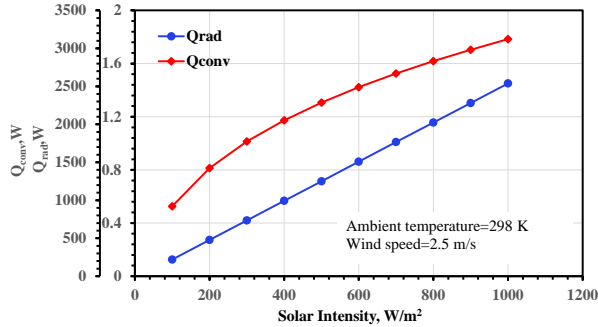


Figure 9. Variation of convection and radiation heat losses against the solar intensity.

The relationships between heat loss and conduction heat against solar intensity are depicted in Fig. 10. As can be seen in the graph, an increase in sun intensity leads to an increase in the solar concentrator's heat loss and conduction heat rate. Thermal losses change during the day due to a variety of factors, including solar irradiation, wind speed, which adds to convection losses, and ambient temperatures. The fluctuation in conduction losses inside the receiver over time is seen in the graph below. The heat transmission to the environment by the flow of air inside the receiver is referred to as convection losses. The useful heat and receiver heat of the concentrator receiver dish is calculated by Eqs. (1) and (2), respectively.

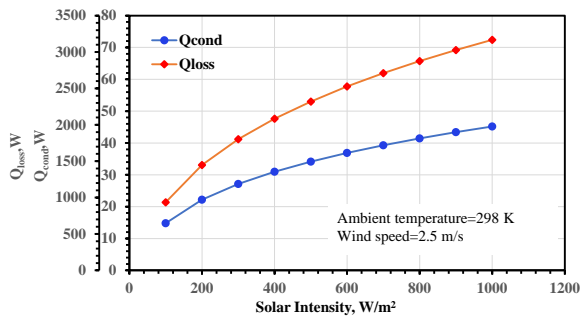


Figure 10. Variation of loss and conduction of heat against the solar intensity

In addition, Fig. 11 illustrates the useful heat rate and receiver heat rate of solar dish collectors against solar intensity for a range of 100-1000 W/m<sup>2</sup> for a constant ambient

temperature of 298 K and wind speed of 2.5 m/s. It can be seen from the figure that the useful heat rate and receiver heat rate of solar dish collector is increased when the solar irradiance increases too. This can be explained by the solar irradiance impact on the solar dish receiver heat transfer rate which is an indicator for enhancing the efficiency of the solar dish collectors. This occurs as a result of an increase in ambient temperature caused by the impact of solar radiation intensity, and as a result, thermal storage increases rapidly, increasing the quantity of usable or receiver heat rate.

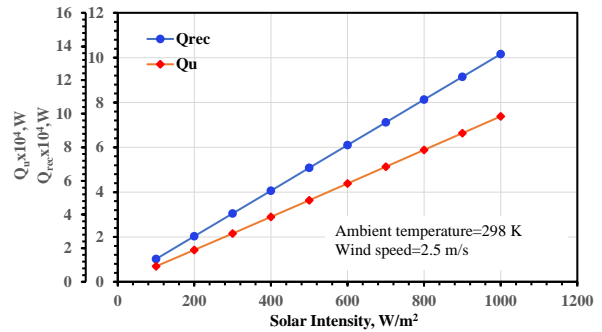


Figure 11. Variation of useful and receiver heat against the solar intensity.

Figure 12 shows the convection and radiation heat rate of the receiver versus ambient temperature at a constant sun intensity of 1000 W/m<sup>2</sup> and a wind speed of 2.5 m/s. As can be observed in the graph, the receiver heat convection decreases fast as the ambient temperature rises. Furthermore, with an increase in ambient air temperature, the receiver's radiation heat rate remains constant. The heat transfer rate via convection is significantly influenced by ambient air temperature, whereas the heat transfer rate via radiation is unaffected.

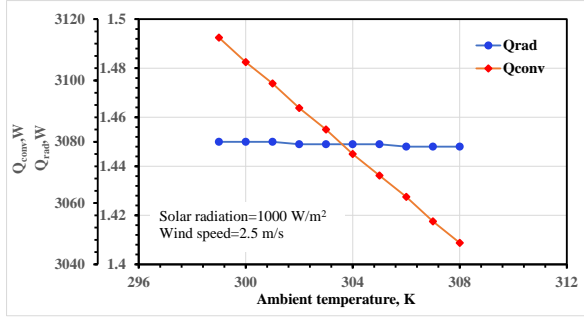


Figure 12. Variation of convection and radiation heat losses against the ambient temperature.

Figure 13 depicts the total heat losses and heat conduction heat loss against the ambient temperature. As can be seen from Fig. 13, the lower the ambient temperature, the higher the thermal losses. That is due to that: increasing the ambient air temperature results in increasing the temperature difference between the operational receiver temperature and weather air temperature and thus decreasing the total thermal losses of the receiver. The results demonstrated in Fig. 13, for the SDC at ambient air temperature values between 298 and 208 K, reveal that the total heat losses of the receiver are between 3.16 and 3.09 kW, when solar radiation intensity is 1000 W/m<sup>2</sup> and wind speed is 2.5 m/s. Moreover, it is clear that the conduction heat loss has an insignificant fraction of the receiver total losses, which is estimated between 0.0452 and 0.0443 kW.

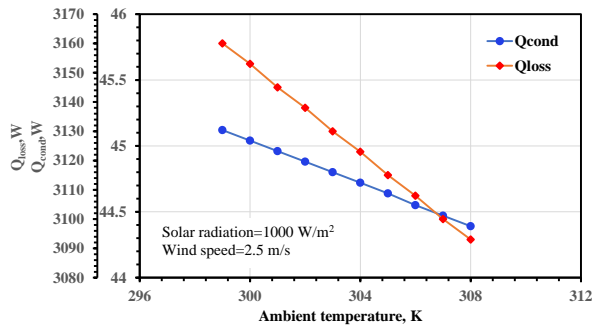


Figure 13. Variation of loss and conduction heat against ambient temperature.

The relationship between the amount of useful heat rate and the amount of receiver heat rate with ambient air temperature is shown in Fig. 14 with an intensity of solar radiation of 1000 W/m<sup>2</sup> and a wind speed of 2.5 m/s. The figure shows that the ambient air temperatures have a slight effect on the receiver's useful heat transfer rate, while it has no effect on the receiver's heat rate for the same reason highlighted above.

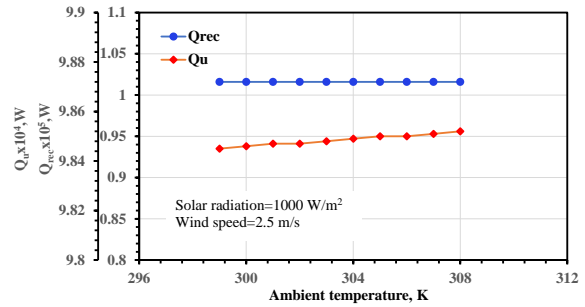


Figure 14. Variation of useful and receiver heat against ambient temperature

### 3.3 Productivity of the MED unit

Figure 13 shows the variation of useful energy with the total distilled water produced using five multi-effect evaporators. The distilled water increases with the increase of useful energy. This is due to the increase in radiation intensity which affected the quantity of useful energy during the daytime.

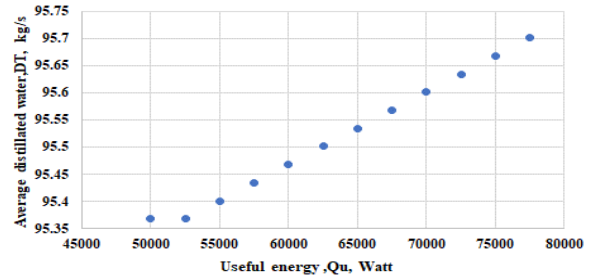


Figure 15. Variation of useful energy versus average total distilled water.

#### 4. Conclusions

A numerical accurate tool is needed to develop and simulate various designs for multi-effect desalination (MED) facilities, under various operating conditions. This investigation concerned a theoretical evaluation of the performance of a solar dish concentrator (SDC) integrated with a MED unit for desalting water. In this work, the performance of a solar dish concentrator (SDC) combined with a MED unit for desalinating water was theoretically evaluated. The proposed SDC/MED system is simulated using MATLAB software, and the performance of the system is examined for Tianjin city, China. The analyzed SDC/MED system's daily, monthly, and yearly performance levels are examined. The following are the primary conclusions:

1. The direct sun radiation intensity substantially impacts the receiver's effective energy output.
2. When the wind speed stays within a range of up to 3.0 m/s, the system performance is noticeably increased; nevertheless, the ambient temperature has an insignificant impact on the system performance.
3. The combined SDC/MED system has an overall efficiency of 80%.
4. The integration of SDC with MED unit achieves average productivity of 95.5 kg/s, a specific cooling water flow rate of 1.689, and an overall performance ratio of 223.3.
5. The total freshwater productivity rate increases by increasing the useful heat gain of the solar receiver.
6. The solar MED distiller system's receiver convection and radiation heat losses are more sensitive to ambient air temperature and direct sun irradiation.

#### References

- [1] R. Almodfer, M.E. Zayed, M.A. Elaziz, M.M. Aboelmaaref, M. Mudhsh, A.H. Elsheikh, Modeling of a solar-powered thermoelectric air-conditioning system using a random vector functional link network integrated with jellyfish search algorithm, *Case Studies in Thermal Engineering*; 31 (2022) 101797
- [2] Liu G, Liu J, E J, Li Y, Zhang Z, Chen J, et al. Effects of different sizes and dispatch strategies of thermal energy storage on solar energy usage ability of solar thermal power plant. *Appl Therm Eng* 2019;156:14–22.
- [3] M. M. Aboelmaaref, M. E. Zayed, J. Zhao, W. Li, A. A. Askalany, M. S. Ahmed, E. S. Ali. Hybrid solar desalination systems driven by the parabolic trough and parabolic dish CSP technologies: Technology categorization, thermodynamic performance, and economical assessment. *Energy Conversion and Management*; 220 (2020) 113103
- [4] Jamil MA, Elmutasim SM, Zubair SM. Exergo-economic analysis of a hybrid humidification dehumidification reverse osmosis (HDH-RO) system operating under different retrofits. *Energy Convers Manage* 2018;158:286–97.
- [5] Khanjanpour MH, Javadi AA. Optimization of a Horizontal Axis Tidal (HAT) turbine for powering a Reverse Osmosis (RO) desalination system using Computational Fluid Dynamics (CFD) and Taguchi method. *Energy Convers Manage* 2021;231:113833.
- [6] Koutsakos E, Delaisse G, van der Wal W. Successful antiscalant field trial – optimization at higher pH and seawater temperature - Larnaca Desalination Plant. *Desalin Water Treat* 2010;13:217–25.
- [7] Shalaby SM, Sharshir SW, Kabeel AE, Kandeal AW, Abosheisha HF, Abdelgaied M, et al. Reverse osmosis desalination systems powered by solar energy: Preheating techniques and brine disposal

challenges – A detailed review. *Energy Convers Manage* 2022;251:114971.

[8] Al-Dafaie A.M.A., Dahdolan M.d.-E., Al-Nimr M.d.A. Utilizing the heat rejected from a solar dish Stirling engine in potable water production [J]. *Solar Energy*, 2016, 136: 317-326

[9] M. E. Zayed, J. Zhao, A.H. Elsheikh, W. Li, S. Sadek, M.M. Aboelmaaref. A comprehensive review on Dish/Stirling concentrated solar power systems: Design, optical and geometrical analyses, thermal performance assessment, and applications. *Journal of Cleaner Production*. (2020) 124664.

[10] Rafiei A., Alsagri A.S., Mahadzir S., et al. Thermal analysis of a hybrid solar desalination system using various shapes of cavity receiver: Cubical, cylindrical, and hemispherical [J]. *Energy Conversion and Management*, 2019, 198: 111861.

[11] Mehrpooya M., Ghorbani B., Hosseini S.S. Thermodynamic and economic evaluation of a novel concentrated solar power system integrated with absorption refrigeration and desalination cycles [J]. *Energy Conversion and Management*, 2018, 175: 337-356.

[12] Voutchkov N. Energy use for membrane seawater desalination – current status and trends. *Desalination* 2018;431:2–14.

[13] Koutsou CP, Kritikos E, Karabelas AJ, Kostoglou M. Analysis of temperature effects on the specific energy consumption in reverse osmosis desalination processes. *Desalination* 2020;476:114213

[14] M. E. Zayed, J. Zhao, A.H. Elsheikh, W. Li, M. A. Elaziz. Optimal design parameters and performance optimization of thermodynamically balanced dish/Stirling concentrated solar power system using multi-objective particle swarm optimization, *Applied Thermal Engineering*; 178 (2020) 115539.

[15] Hills S, Dana S, Wang H. Dynamic modeling and simulation of nuclear hybrid

energy systems using freeze desalination and reverse osmosis for clean water production. *Energy Convers Manage* 2021;247:114724.

[16] Shamel MM, Chung OT. Drinking water from desalination of seawater: optimization of reverse osmosis system operating parameters. *J Eng Sc Technol* 2006;1(2):203–11.

[17] Atab MS, Smallbone AJ, Roskilly AP. An operational and economic study of a reverse osmosis desalination system for potable water and land irrigation. *Desalination* 2016;397:174–84.

[18] Al-Zahrani A, Orfi J, Al-Suhaibani Z, Salim B, Al-Ansary H. Thermodynamic analysis of a reverse osmosis desalination unit with energy recovery system. *Procedia Eng* 2012;33:404–14.

[19] M. E. Zayed, J. Zhao, W. Li, M.A. Elaziz, A.H. Elsheikh, S. Zhong, D. Yousri. Predicting the performance of solar dish Stirling power plant using a hybrid random vector functional link/chimp optimization model. *Solar Energy*; (2021), 222, 1-17.

[20] El-Emam RS, Dincer I. Thermodynamic and thermoeconomic analyses of seawater reverse osmosis desalination plant with energy recovery. *Energy* 2014;64:154–63.

[21] Sagade AA, Mawire A, Belgasim B, Tawfik MA, Sagade NA. Experimental performance evaluation of a parabolic dish solar geyser using a generalized approach for decentralized applications. *Sustainable Energy Technol Assess* 2021; 47:101454.

[22] Sandoval OR, Caetano BCB, Ungaretti M, Garcia JJ, Molina VR. Modelling simulation and thermal analysis of a solar dish/Stirling system: a case study in Natal. Brazil *Energy Convers Manage* 2019;181:189–201.

[23] Bellos E, Bousi E, Tzivanidis C, Pavlovic S. Optical and thermal analysis of different cavity receiver designs for solar dish concentrators. *Energy Conversion and Management: X* 2019;2:100013.

- [٣٤] Loni R, Asli-Ardeh EA, Ghobadian B, Bellos E, Le Roux WG. Numerical comparison of a solar dish concentrator with different cavity receivers and working fluids. *J Cleaner Prod* 2018;198:1013–30.
- [٣٥] Pavlovic S, Daabo AM, Bellos E, Stefanovic V, Mahmoud S, Al-Dadah RK. Experimental and numerical investigation on the optical and thermal performance of solar parabolic dish and corrugated spiral cavity receiver. *J Cleaner Prod* 2017; 150:75–92.
- [٣٦] M. E. Zayed, J. Zhao, W. Li, A.H. Elsheikh, M.A. Elaziz. A hybrid adaptive neuro-fuzzy inference system integrated with an equilibrium optimizer algorithm for predicting the energetic performance of solar dish collector. *Energy*; (2021); 235, 121289.
- [٣٧] Z. Li, D. Tang, J. Du, T. Li, Study on the radiation flux and temperature distributions of the concentrator–receiver system in a solar dish/Stirling power facility, *Appl. Therm. Eng.* 31 (2011) 1780–1789.
- [٣٨] Yan, J., Peng, Y.D., Cheng, Z.R., Liu, F.M., Tang, X.H., 2017. Design and implementation of a 38 kW dish-Stirling concentrated solar power system. *IOP Conference Series: Earth and Environmental Science*, 93., pp. 012052.
- [٣٩] W.B. Stine, R.W. Harrigan, *Solar energy fundamentals and design with computer applications*, Willy, 1985.
- [٤٠] Zayed, M.E., Zhao, J., Li, W., Elsheikh, A.H., Zhao, Z., Khalil, A., Li, H., 2020. Performance prediction and techno-economic analysis of solar dish/Stirling system for electricity generation. *Appl. Therm. Eng.* 164, 114427.
- [31] Zayed, M. E., Zhao, J., Elsheikh, A. H., Zhao, Z., Zhong, S., & Kabeel, A. E. (2021). Comprehensive parametric analysis, design and performance assessment of a solar dish/Stirling system. *Process Safety and Environmental Protection*, 146, 276-291.
- [32] Gamal. B. Abdelaziz, M.A. Dahab, M.E. Omara, S.W. Sharshir, Ashraf Mimi Elsaid, E.M.S. El-Said, Humidification dehumidification saline water desalination system utilizing high-frequency ultrasonic humidifier and solar heated air stream, *Thermal Science and Engineering Progress* (2021) 101144.
- [33] Mendoza Castellanos, L.S., Carrillo Caballero, G.E., Melian Cobas, V.R., Silva Lora, E.E., Martinez Reyes, A.M., 2017. Mathematical modeling of the geometrical sizing and thermal performance of a dish/Stirling system for power generation. *Renew. Energy* 107, 23–35.
- [34] Steinfeld, A., Schubnell, M., 1993. Optimum aperture size and operating temperature of a solar cavity receiver. *Sol. Energy* 50, 19–25.
- [35] Steinfeld A, P.R., 2003. Solar thermochemical process technology. *Encycl. Phys. Sci. Technol.*, 237–256.
- [36] Carrillo Caballero, G.E., Mendoza, L.S., Martinez, A.M., Silva, E.E., Melian, V.R., Ven-turini, O.J., del Olmo, O.A., 2017. Optimization of a dish Stirling system working with DIR-type receiver using multi-objective techniques. *Appl. Energy* 204,271–286.
- [37] L.S. Mendoza Castellanos, A.L. Galindo Noguera, G.E. Carrillo Caballero, A.L. De Souza, V.R. Melian Cobas, E.E. Silva Lora, O.J. Venturini, Experimental analysis and numerical validation of the solar Dish/Stirling system connected to the electric grid, *Renew. Energy* 135 (2019) 259–265.
- [38] R.Y. Ma, Wind effects on convective heat loss from a cavity receiver for a parabolic concentrating solar collector, Sandia (1993).
- [39] L. Ma, Y. Li, J. Wang, S. Li, J. Zhao, W. Li, M.E. Zayed, Q. Shao, M. Sun, A thermal dissipation correction method for in-situ soil thermal response test: experiment and simulation under multi-operation conditions, *Energy Build.* 194 (2019) 218–231.
- [40] M.E. Zayed, J. Zhao, Y. Du, A.E. Kabeel, S.M. Shalaby, Factors affecting the

thermal performance of the flat plate solar collector using nanofluids: a review, *Sol. Energy* 182 (2019) 382–396.

[41] M.E. Zayed, J. Zhao, A.H. Elsheikh, F.A. Hammad, L. Ma, Y. Du, A.E. Kabeel, S.M. Shalaby, Applications of cascaded phase change materials in solar water collector storage tanks: a review, *Sol. Energy Mater. Sol. Cells* 199 (2019) 24–49.

[42] V.T. Morgan, The overall convective heat transfer from smooth circular cylinders, in: T.F. Irvine, J.P. Hartnett (Eds.), *Advances in Heat Transfer*, Elsevier, 1975, pp.199–264.

[43] Al-Mutaz IS, Wazeer I. Development of a steady-state mathematical model for MEE-TVC desalination plants. *Desalination* 2014;351:9–18.

[44] M.A. Darwish, Hassan K. Abdulrahim, Feed water arrangements in a multi-effect desalting system, *Desalination* 228 (2008) 30–54.

[45] M. Abd Elaziz, S. Senthilraja, M.E. Zayed, A.H. Elsheikh, R.R. Mostafa, S. Lu, A new random vector functional link integrated with mayfly optimization algorithm for performance prediction of solar photovoltaic thermal collector combined with electrolytic hydrogen production system, *Applied Thermal Engineering*,193 (2021) 117055..